

## Swelling and shrinking of two opposing polyelectrolyte brushes

Mingyu Duan<sup>1</sup> and Guang Chen<sup>1\*</sup>*Department of Advanced Manufacturing and Robotics, College of Engineering, Peking University, Beijing 100871, People's Republic of China*
 (Received 6 July 2022; revised 24 August 2022; accepted 18 January 2023; published 10 February 2023)

Salt concentration and confinement effects affect the configuration of polyelectrolyte (PE) brushes due to electrostatic interactions. In this work, we develop a new theoretical model to analyze the electrostatics and swelling-shrinking behavior of two opposing PE brushes. By comparing three length scales, i.e., equilibrium brush height, separation distance, and Debye length, we obtain distinct scaling laws for brush height in different regimes. We provide explanations for the anomalous shrinkage of the PE brush with added salt reported in experiments and simulations, the applicability of the homogeneous brush assumption, and the confinement effect on the brush height. Our model can be used to shed light on the configuration and functionalities of PE-grafted interfaces, which play important roles in ion selective membranes and organism lubrication. We also anticipate that our method will be useful to understand the functionalities of other charged soft matter systems, such as hydrogel swelling and colloidal stability.

DOI: [10.1103/PhysRevE.107.024502](https://doi.org/10.1103/PhysRevE.107.024502)

### I. INTRODUCTION

Polyelectrolyte (PE) brushes are formed by PE chains that are densely grafted to solid-liquid interfaces [1–3]. Due to the electrostatic interactions among PE chains and their surrounding electrolyte ions, PE brush configurations change with ambient factors such as salt concentration [4–7] and confinement effects [8]. The swelling-shrinking behavior of a PE brush under stimulation of the changes in salt concentration or pH value enables its applications in microfluidics and medicine, such as the switching of ionic valves [9–12] and encapsulation and release of targeted drugs [13–16]. The electrostatic interactions between two opposing PE brushes, along with their stimuli-responsive configuration, play important roles in the lubrication properties of the functionalized interfaces [17–20].

Scaling theories have been developed to characterize the impact of salt concentration  $n_s$  on the PE brush height  $H$ . The salted brush (SB) regime predicts  $H \propto n_s^{-1/3}$  when salt concentration far exceeds the local counterion concentrations inside the brush layer. The osmotic brush (OsB) regime and the Pincus brush (PB) regime state that  $H$  is independent of  $n_s$  under a salt-free assumption [21–23]. These classical scaling laws have been verified experimentally [5,6,24,25].

However, there exists several puzzles on the PE brush configuration: (i) Recent experiments and molecular dynamics (MD) simulations have shown anomalous shrinkage of PE brushes with added salt of  $H \propto n_s^{-0.15}$  and  $H \propto n_s^{-0.17}$ , which cannot be captured by the SB regime [26,27]. (ii) The applicability of the homogeneous brush assumption made by the classical scaling theories (i.e., step function monomer profile) has been questioned over the years [4,6], yet there is no definitive explanation. (iii) When two opposing brushes are brought

into close contact and remain noninterpenetrating, the interaction between brushes (i.e., confinement effect) becomes non-negligible, especially in the scenarios of lubrication [20] in medical or biological applications and measurements of the brush height using surface forces apparatus (SFA) [8].

In this work, we propose a theoretical model to characterize the impact of salt and confinement effect on the configuration of two opposing PE brushes. We identify three length scales, i.e., equilibrium brush height  $H$ , separation distance  $D$ , and Debye length  $\lambda$ , and asymptotically obtain three scaling regimes for the brush height. Finally, we compare our model with the classical scaling theories, MD simulations and experiments, and attempt to explain the aforementioned puzzles.

### II. THEORY

We model two opposing PE brushes that are grafted to planar substrates in a polar solvent, with bulk salt concentration  $n_s$ , brush height  $H$ , and separation distance between the substrates  $2D$ , where  $H < D$ , as illustrated in Fig. 1(a). For either PE brush, the PE chains are identical with the same polymerization  $N_p$  ( $N_p \gg 1$ ), monomer size  $a$ , grafting distance  $\xi$ , and charge fraction  $\varphi$ . The PE chains on the substrates are densely grafted and attain a brushlike configuration, which requires  $\xi \leq H$ . Following the Alexander-de Gennes polymer brush model [28–30], we model the PE brushes as closely packed blobs of size  $\xi$ , and the monomers are assumed to be homogeneously distributed and dissociated inside the brushes, i.e., monomer density  $n_p = N_p/(\xi^2 H)$  and  $\varphi$  are constants.

The total free energy of a PE chain and its surrounding electrolyte ions shown in Fig. 1(b) is [31,32]

$$F = F_{\text{els}} + F_{\text{EV}} + F_{\text{elec}}, \quad (1)$$

where  $F_{\text{els}} = k_B T H^2 / (a^2 N_p)$  and  $F_{\text{EV}} = k_B T \nu N_p^2 / (\xi^2 H)$  are, respectively, the elastic energy and the excluded volume energy following the Alexander-de Gennes model [28–30],  $F_{\text{elec}}$

\*Corresponding author: [guangc@pku.edu.cn](mailto:guangc@pku.edu.cn)

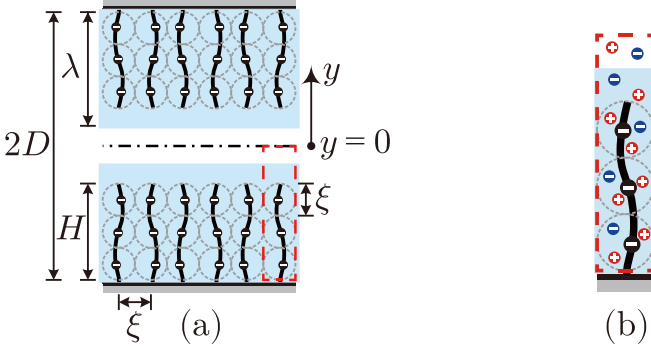


FIG. 1. Schematics of (a) two opposing PE brushes and (b) a PE chain and its surrounding electrolyte ions.

is the electrostatic energy,  $\nu = (1 - 2\chi)a^3$  is the excluded volume parameter, and  $\chi$  is the Flory parameter.

Considering negatively charged monomers and monovalent electrolyte ions ( $z_{\pm} = \pm 1$ ), the electrostatic energy is [3]

$$\begin{aligned} \frac{F_{\text{elec}}}{k_B T} = & -\xi^2 \int_{-D}^{-D+H} \frac{e\psi}{k_B T} \frac{N_p \varphi}{\xi^2 H} dy - \xi^2 \int_{-D}^0 \frac{\epsilon_0 \epsilon_r}{2k_B T} \left| \frac{d\psi}{dy} \right|^2 dy \\ & + \xi^2 \int_{-D}^0 \sum \left\{ \frac{e\psi}{k_B T} z_i n_i + n_{i,\infty} + n_i \left[ \ln \left( \frac{n_i}{n_{i,\infty}} \right) - 1 \right] \right\} dy, \end{aligned} \quad (2)$$

where  $\psi$  is the electrostatic potential relative to a reference  $\psi = 0$  in the bulk,  $\epsilon_0$  is the vacuum permittivity,  $\epsilon_r$  is the relative dielectric constant of water, and  $n_i$  and  $n_{i,\infty} = n_s$  ( $i = \pm$ ) are the local and bulk ion concentrations, respectively [31,32]. Here, the first term is the electrostatic energy of one PE chain, the second term is the self-energy of the electric field, and the third term consists of the Coulomb interactions and the entropy of mixing the electrolyte ions. Each term of the electrostatic energy in Eq. (2) varies with the electrostatic potential  $\psi$ , the local ion concentration  $n_{\pm}$ , and the brush height  $H$  at equilibrium, and is eventually a function of the bulk salt concentration  $n_s$ .

Minimizing  $F_{\text{elec}}$  with respect to  $\psi$  and  $n_{\pm}$  respectively leads to the Poisson equation and Boltzmann distribution,

$$\frac{d^2 \psi}{dy^2} = \frac{e(n_- - n_+ + \frac{N_p \varphi}{\xi^2 H})}{\epsilon_0 \epsilon_r}, \quad \text{for } -D \leq y \leq -D + H, \quad (3a)$$

$$\frac{d^2 \psi}{dy^2} = \frac{e(n_- - n_+)}{\epsilon_0 \epsilon_r}, \quad \text{for } -D + H \leq y \leq 0, \quad (3b)$$

$$n_{\pm} = n_s \exp\left(\mp \frac{e\psi}{k_B T}\right), \quad \text{for } -D \leq y \leq 0. \quad (3c)$$

We assume that the substrate at  $y = \pm D$  is neutral, and the electrostatic potential is continuous at  $y = -D + H$ :

$$\left. \frac{d\psi}{dy} \right|_{y=-D} = 0, \quad (4a)$$

$$\psi|_{y=(-D+H)^+} = \psi|_{y=(-D+H)^-}, \quad (4b)$$

$$\left. \frac{d\psi}{dy} \right|_{y=(-D+H)^+} = \left. \frac{d\psi}{dy} \right|_{y=(-D+H)^-}. \quad (4c)$$

A symmetric boundary condition is used at  $y = 0$ :

$$\left. \frac{d\psi}{dy} \right|_{y=0} = 0. \quad (5)$$

Then the numerical solution of the brush height  $H$  at equilibrium with respect to a minimum free energy  $F$  can be obtained using Eqs. (1)–(5).

### III. RESULTS

Analytic solutions for Eq. (3) are obtained within the Debye-Hückel (DH) limit, i.e.,  $|\Psi| \ll 1$  [where  $\Psi = e\psi/(k_B T)$  is the dimensionless electrostatic potential]:

$$\Psi \approx -\frac{N_p \varphi}{\xi^2 H 2n_s} \left[ 1 - \frac{\sinh\left(\frac{D-H}{\lambda}\right)}{\sinh\left(\frac{D}{\lambda}\right)} \cosh\left(\frac{y+D}{\lambda}\right) \right], \quad \text{for } -D \leq y \leq -D + H, \quad (6a)$$

$$\Psi \approx -\frac{N_p \varphi}{\xi^2 H 2n_s} \frac{\sinh\left(\frac{H}{\lambda}\right)}{\sinh\left(\frac{D}{\lambda}\right)} \cosh\left(\frac{y}{\lambda}\right), \quad \text{for } -D + H \leq y \leq 0, \quad (6b)$$

where  $\lambda = \sqrt{\epsilon_0 \epsilon_r k_B T / (2n_s e^2)}$  is the Debye length. Note that Eq. (6) is consistent with Ref. [33], which assumes that the dissociated groups of valence were homogeneously distributed inside the brush, i.e.,  $n_p$  and  $\varphi$  are constants. However,  $\Psi$  in Eq. (6) is a function of  $y$ . The spatial variation of  $\Psi$  may cause nonhomogeneous dissociation and distribution of the monomers, which violates the homogeneous brush assumption.

To address this concern, we identify three important length scales, i.e., the equilibrium brush height  $H$ , the separation distance  $D$ , and the Debye length  $\lambda$ , and obtain asymptotic approximations for Eq. (6a) as

$$|\Psi| \approx \frac{N_p \varphi}{\xi^2 H 2n_s}, \quad \text{for } \lambda \ll H \ll D, \quad (7a)$$

$$|\Psi| \approx \frac{N_p \varphi}{\xi^2 \lambda 2n_s}, \quad \text{for } H \ll \lambda \ll D, \quad (7b)$$

$$|\Psi| \approx \frac{N_p \varphi}{\xi^2 D 2n_s}, \quad \text{for } H < D \ll \lambda. \quad (7c)$$

Therefore the homogeneous brush assumption is appropriate when  $\lambda$  and  $H$  are of different orders of magnitude since  $\Psi$  is approximately constant in Eq. (7).

Now considering the PE brushes in a  $\theta$ -solvent, i.e.,  $\chi = 0.5$ , we obtain the total free energy when  $|\Psi| \ll 1$  using Eqs. (1)–(3) and (6):

$$\frac{F}{k_B T} \approx \frac{H^2}{a^2 N_p} + \frac{N_p^2 \varphi^2}{\xi^2 H 4n_s} \left[ 1 - \frac{\lambda}{H} \frac{\sinh\left(\frac{H}{\lambda}\right) \sinh\left(\frac{D-H}{\lambda}\right)}{\sinh\left(\frac{D}{\lambda}\right)} \right]. \quad (8)$$

Minimizing  $F$  with respect to  $H$  yields the analytic solution for the equilibrium brush height,

$$\begin{aligned} \left( \frac{H}{aN_p} \right)^3 \approx & \frac{\varphi^2}{4} \left( \frac{a}{\xi} \right)^2 \frac{1}{n_s a^3} \frac{\sinh\left(\frac{D-H}{\lambda}\right)}{\sinh\left(\frac{D}{\lambda}\right)} \\ & \times \left[ \cosh\left(\frac{H}{\lambda}\right) - \frac{\lambda}{H} \sinh\left(\frac{H}{\lambda}\right) \right], \end{aligned} \quad (9)$$

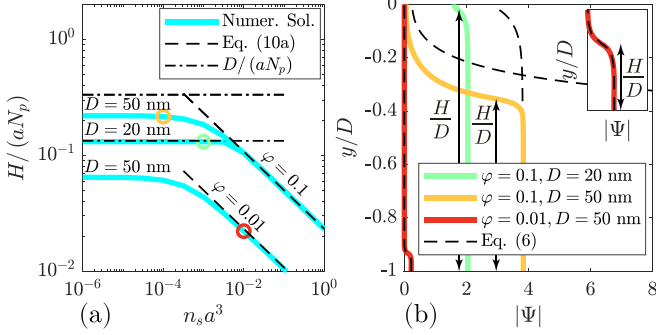


FIG. 2. (a)  $H/(aN_p)$  as a function of  $n_s a^3$  for various  $\varphi$  and  $D$ , where the circles mark  $H/(aN_p)$  at  $n_s a^3 = 10^{-4}, 10^{-3}, 10^{-2}$ . (b) Spatial distributions of  $\Psi$  for specific  $H/(aN_p)$  marked in (a). Parameters used are  $\epsilon_0 = 8.8 \times 10^{-12}$  F/m,  $\epsilon_r = 80$ ,  $T = 300$  K,  $a = 0.3$  nm,  $N_p = 500$ ,  $\xi/a = 10$ , and  $\chi = 0.5$ .

which can be simplified to

$$\frac{H}{aN_p} \approx \frac{1}{2} \varphi^3 \left( \frac{a}{\xi} \right)^{2/3} (n_s a^3)^{-1/3}, \quad \text{for } \lambda \ll H \ll D, \quad (10a)$$

$$\frac{H}{aN_p} \approx \frac{2\pi}{3} N_p^2 \varphi^2 \left( \frac{a}{\xi} \right)^2 \frac{\ell_B}{a}, \quad \text{for } H \ll \lambda \ll D, \quad (10b)$$

$$\frac{H}{aN_p} \approx \frac{2\pi \ell_B a N_p^2 \varphi^2 D}{2\pi \ell_B a^2 N_p^3 \varphi^2 + 3D\xi^2}, \quad \text{for } H < D \ll \lambda, \quad (10c)$$

where  $\ell_B = e^2/(4\pi\epsilon_0\epsilon_r k_B T)$  is the Bjerrum length. Note that the analytic predictions, i.e., Eqs. (10a)–(10c), are valid within the DH limit ( $|\Psi| \ll 1$ ) and the brushlike configuration ( $\xi \leq H$ ). Equations (10a) and (10b) agree with the classical SB regime and PB regime, respectively [21–23]. Equation (10c) yields  $H \approx D$  at small separation distance  $D \ll 2\pi N_p^3 \varphi^2 a^2 \ell_B / (3\xi^2)$ .

The numerical solutions for the dimensionless equilibrium brush height  $H/(aN_p)$  with dimensionless added salt  $n_s a^3$  for various charge fractions  $\varphi$  and separation distances  $D$  are plotted in Fig. 2(a). The results for  $H/(aN_p)$  show plateaus at small  $n_s a^3$  and then decrease with  $n_s$  increase. The brush height becomes lower with a smaller  $\varphi$ . The decrease of  $H/(aN_p)$  at large  $n_s a^3$  (where  $\lambda \ll H$ ) is captured by our prediction Eq. (10a) (which agrees with the SB regime [21,23]). The two plateaus for  $H/(aN_p)$  at small  $n_s a^3$  for  $D = 50$  nm cannot be captured by Eq. (10b) or (10c), since the corresponding  $\Psi$  goes beyond the DH limit [see Fig. 2(b)]. We cannot justify these plateaus as the OsB regime either, since we do not make the salt-free assumption as used in the classical OsB regime [21,22]. The plateau for  $H/(aN_p)$  at small  $n_s a^3$  for  $D = 20$  nm is captured by  $D/(aN_p)$ , which suggests that the confinement effect on  $H$  is important at low salt concentration and small separation distance.

The dimensionless potential distributions of  $|\Psi|$  with various  $\varphi$  and  $D$  are plotted in Fig. 2(b), where the brush heights  $H/D$  marked by the arrows correspond to the specific  $H/(aN_p)$  marked by the circles in Fig. 2(a). Note that  $\Psi$  shown in Fig. 2(b) is approximately constant inside the brush, which is consistent with our discussions on the homogeneous brush assumption and Eq. (7).

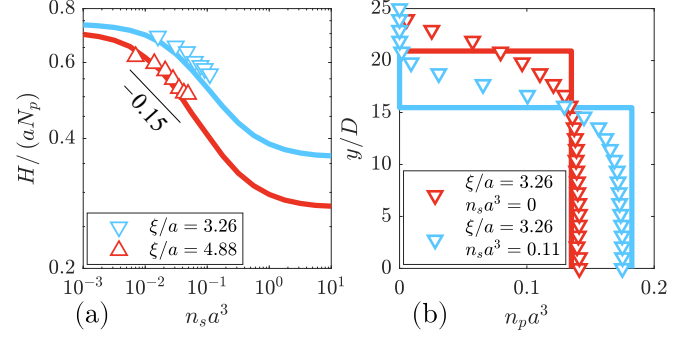


FIG. 3. (a) Comparison between the MD simulations (scatters) [26] and our numerical solutions (solid lines) for  $H/(aN_p)$  as a function of  $n_s$  with identical parameters for various  $\xi$  and  $D$ . (b) Comparisons between the MD simulations (scatters) [26] and our numerical solutions under the homogeneous brush assumption (solid lines) for monomer density profile  $n_p a^3$  as a function of  $y/a$  for various  $n_s a^3$ . Here, we use the solution for the brush height at  $n_s a^3 = 10^{-3}$  to approximate the salt-free condition, i.e.,  $n_s a^3 = 0$ . Parameters used are  $a = \ell_B = 0.7$  nm,  $N_p = 30$ ,  $\varphi = 1$ ,  $\chi = 0$ , and  $D = 2aN_p$ .

#### IV. DISCUSSIONS

With our numerical predictions and scaling laws for the brush height and the potential distribution, we can now provide explanations for the aforementioned puzzles on the PE brush configuration.

(i) *Anomalous shrinkage of the brush height.* Variations of  $H/(aN_p)$  with  $n_s a^3$  predicted by previous MD simulations [26] are plotted in Fig. 3(a). It is claimed that the best fitting power law for the data points is  $H \propto n_s^{-0.15}$ , which deviates far from the classical SB regime  $H \propto n_s^{-1/3}$  [26]. Here, we fit the data with our numerical prediction for the brush height in solid lines as shown in Fig. 3(a), where we consider the brushes in a good solvent with  $\chi = 0$ . Comparing with our prediction for  $H/(aN_p)$  at large  $n_s a^3$  in Fig. 2(a), where  $\chi = 0.5$  and  $F_{EV} = 0$ , we note that here the excluded volume energy is the key factor of the anomalous shrinkage of the brush. It is also possible that the anomalous shrinkage of the brush is due to the inhomogeneity of the ion distribution among the PE chains, though there is no definitive explanation [34,35]. Please note that the inhomogeneity of the ion distribution is beyond the scope of the present model as well as the classical scaling theories. We will incorporate the effect of local ion distribution in our future work.

(ii) *Monomer density profile.* The monomer density profiles  $n_p a^3$  reported in [26] are plotted in Fig. 3(b). The corresponding Debye lengths and brush heights used in Ref. [26] for  $n_s a^3 = 0$  and  $n_s a^3 = 0.11$  correspond to  $\lambda \rightarrow +\infty, H = 15.75$  nm and  $\lambda = 0.42$  nm,  $H = 12.25$  nm, with our notation, respectively. It can be seen that  $\lambda$  and  $H$  differ by more than one order of magnitude, and the monomer density inside the brush is approximately constant. Our numerical solutions for the dimensionless monomer density  $n_p a^3 = N_p a^3 / (\xi^2 H)$  under the homogeneous brush assumption (i.e., step function monomer profile) also quantitatively fit well with the MD simulations. Note that our predictions for  $\Psi$  inside the brush in Fig. 2(b) show similar profiles as the MD data in Fig. 3(b),

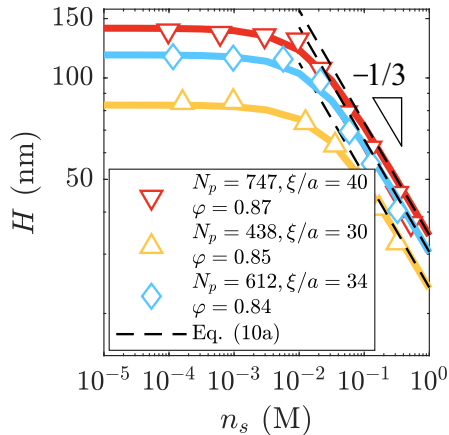


FIG. 4. Comparison between the measurements (scatters) [24] and our numerical solutions (solid lines) for  $H$  as a function of  $n_s$  with identical parameters for various  $N_p$ ,  $\xi$ , and  $\varphi$ . Parameters used are  $\epsilon_0 = 8.8 \times 10^{-12}$  F/m,  $\epsilon_r = 80$ ,  $T = 300$  K,  $a = 0.29$  nm,  $\chi = 0.5$ , and  $D = 300$  nm.

which is approximately constant inside the brush. The homogeneous brush assumption is consistent with the spatial distribution of  $\Psi$  only in certain regimes when  $\lambda$  and  $H$  are not comparable ( $\lambda \ll H$  or  $\lambda \gg H$ ). In other words, the homogeneous brush assumption is invalid when  $H \approx \lambda$ , although our model can give the corresponding solutions under this scenario.

(iii) *Confinement effect in brush height measurements.* The experimental data for  $H$  of two opposing brushes measured by SFA [24] is shown in Fig. 4, in which  $H$  was determined by identifying the separation distance at the first detectable interaction. It is shown that the data follows the classical scaling law  $H \propto n_s^{-1/3}$  at high salt concentration. Accordingly, we use identical parameters as [24] and consider  $\chi = 0.5$  to obtain the numerical predictions for  $H$  in solid lines, which fit well with the experimental measurements. Note that here a larger separation distance  $D = 300$  nm will not change our prediction for the brush height  $H$  at lower salt concentration  $n_s$ , which implies that the confinement effect is weak. However,

other measurements have shown that the two opposing brush heights measured by SFA (i.e., finite  $D$  with our notation) are significantly lower than the single brush height measured by neutron reflectivity (i.e.,  $D \rightarrow \infty$  with our notation) [8]. Although it is possible that the SFA measured the separation distance  $D$  rather than the brush height  $H$ , it is an evidence that the confinement effect of two opposing PE brushes affects the brush configuration.

## V. CONCLUSIONS

We probe the electrostatics and equilibrium brush height of two opposing PE brushes and provide explanations for the aforementioned puzzles on the brush configuration: (i) The anomalous shrinkage of PE brush height with added salt, i.e.,  $H \propto n_s^{-0.15}$  and  $H \propto n_s^{-0.17}$ , observed in experimental measurements and MD simulations, which deviates from the classical salted brush regime  $H \propto n_s^{-1/3}$ , may be caused by the excluded volume energy. (ii) The homogeneous brush assumption is applicable when the brush height  $H$  and the Debye length  $\lambda$  are not comparable, i.e.,  $\lambda \ll H$  or  $\lambda \gg H$  with our notation. (iii) The confinement effect induced by small separation distance  $D$  between two opposing brushes (i.e.,  $D \approx H$  or  $D \approx \lambda$  with our notation) affects the measurement of the brush height by SFA. These remarks rationalize the range of applicability of the classical scaling theories and also provide physical insight for MD simulations and experimental characterizations of PE brushes. We anticipate that our model will be able to predict the PE brush configuration in applications of ionic valves and biomembranes, as well as the lubrication between artificial joint interfaces and organisms [20,33]. The present modeling procedure can also be used to understand the swelling-shrinking nature of other charged soft matter systems such as hydrogel [36] and soil, as well as the stability of colloids [37].

## ACKNOWLEDGMENT

The authors thank Prof. Howard A. Stone and Prof. Ralph H. Colby for helpful discussions.

- [1] S. T. Milner, *Science* **251**, 905 (1991).
- [2] B. Zhao and W. Brittain, *Prog. Polym. Sci.* **25**, 677 (2000).
- [3] S. Das, M. Banik, G. Chen, S. Sinha, and R. Mukherjee, *Soft Matter* **11**, 8550 (2015).
- [4] Y. Mir, P. Auroy, and L. Auvray, *Phys. Rev. Lett.* **75**, 2863 (1995).
- [5] H. Ahrens, S. Förster, and C. A. Helm, *Phys. Rev. Lett.* **81**, 4172 (1998).
- [6] G. Romet-Lemonne, J. Daillant, P. Guenoun, J. Yang, and J. W. Mays, *Phys. Rev. Lett.* **93**, 148301 (2004).
- [7] Y. Mei, K. Lauterbach, M. Hoffmann, O. V. Borisov, M. Ballauff, and A. Jusufi, *Phys. Rev. Lett.* **97**, 158301 (2006).
- [8] J. Yu, J. Mao, G. Yuan, S. Satija, Z. Jiang, W. Chen, and M. Tirrell, *Macromolecules* **49**, 5609 (2016).
- [9] S. Raafatnia, O. A. Hickey, and C. Holm, *Phys. Rev. Lett.* **113**, 238301 (2014).
- [10] G. Chen and S. Das, *J. Phys. Chem. B* **121**, 3130 (2017).
- [11] G. Chen and S. Das, *Electrophoresis* **38**, 720 (2017).
- [12] F. Paratore, E. Boyko, G. V. Kaigala, and M. Bercovici, *Phys. Rev. Lett.* **122**, 224502 (2019).
- [13] Q. Yan and J. J. de Pablo, *Phys. Rev. Lett.* **91**, 018301 (2003).
- [14] Y. Shen, Y. Zhan, J. Tang, P. Xu, P. A. Johnson, M. Radosz, E. A. Van Kirk, and W. J. Murdoch, *AIChE J.* **54**, 2979 (2008).
- [15] L. Zhang, H. P. Bei, Y. Piao, Y. Wang, M. Yang, and X. Zhao, *ChemPhysChem* **19**, 1956 (2018).
- [16] S. N. Innes-Gold, P. A. Pincus, M. J. Stevens, and O. A. Saleh, *Phys. Rev. Lett.* **123**, 187801 (2019).
- [17] U. Raviv, S. Giasson, N. Kampf, J. F. Gohy, R. Jérôme, and J. Klein, *Nature* **425**, 163 (2003).
- [18] J. Zhang, P. M. Lettinga, J. K. G. Dhont, and E. Stiakakis, *Phys. Rev. Lett.* **113**, 268303 (2014).

- [19] E. B. Zhulina and M. Rubinstein, *Macromolecules* **47**, 5825 (2014).
- [20] J. Yu, N. E. Jackson, X. Xu, Y. Morgenstern, Y. Kaufman, M. Ruths, J. J. de Pablo, and M. Tirrell, *Science* **360**, 1434 (2018).
- [21] P. Pincus, *Macromolecules* **24**, 2912 (1991).
- [22] O. V. Borisov, T. M. Birshtein, and E. B. Zhulina, *J. Phys. II* **1**, 521 (1991).
- [23] O. V. Borisov, E. B. Zhulina, and T. M. Birshtein, *Macromolecules* **27**, 4795 (1994).
- [24] M. Balastre, F. Li, P. Schorr, J. Yang, J. W. Mays, and M. V. Tirrell, *Macromolecules* **35**, 9480 (2002).
- [25] B. Lego, W. G. Skene, and S. Giasson, *Macromolecules* **43**, 4384 (2010).
- [26] N. A. Kumar and C. Seidel, *Macromolecules* **38**, 9341 (2005).
- [27] N. Hollingsworth and R. G. Larson, *Polymers* **13**, 812 (2021).
- [28] P. G. de Gennes, *J. Phys. II* **37**, 1445 (1976).
- [29] S. Alexander, *J. Phys. II* **38**, 983 (1977).
- [30] P. G. de Gennes, *Macromolecules* **13**, 1069 (1980).
- [31] G. Chen, A. Perazzo, and H. A. Stone, *Phys. Rev. Lett.* **124**, 177801 (2020).
- [32] G. Chen, A. Perazzo, and H. A. Stone, *J. Rheol.* **65**, 507 (2021).
- [33] H. Ohshima, *Colloid Polym. Sci.* **292**, 431 (2014).
- [34] C. Seidel, *Macromolecules* **36**, 2536 (2003).
- [35] A. Naji, R. R. Netz, and C. Seidel, *Eur. Phys. J. E* **12**, 223 (2003).
- [36] J. Landsgesell, D. Sean, P. Kreissl, K. Szuttor, and C. Holm, *Phys. Rev. Lett.* **122**, 208002 (2019).
- [37] A. P. dos Santos and Y. Levin, *Phys. Rev. Lett.* **106**, 167801 (2011).